JTTEES 5:476-482

Thermal-Sprayed Fe-10Cr-13P-7C Amorphous Coatings Possessing Excellent Corrosion Resistance

K. Kishitake, H. Era, and F. Otsubo

An alloy of Fe-10Cr-13P-7C was thermally sprayed by three different processes: (1) 80 kW low-pressure plasma spraying (LPPS), (2) high-velocity oxyfuel (HVOF) spraying, and (3) 250 kW high-energy plasma spraying (HPS). The as-sprayed coating obtained by the LPPS process was composed of an amorphous phase. In contrast, the as-sprayed coatings obtained by the HVOF and HPS processes were a mixture of amorphous and crystalline phases. The as-sprayed coatings showed a high hardness of 700 DPN. A very fine structure composed of ferrite, carbide, and phosphide was formed, producing a maximum hardness of greater than 1000 DPN in the LPPS coating just after crystallization on tempering. The corrosion resistance of the amorphous coating was superior to a SUS316L stainless steel coating in 1 *N* H_2SO_4 solution and 1 *N* HCl solution. Furthermore, the amorphous coating underwent neither general nor pitting corrosion in 1 *N* HCl solution and 6% $FeCl_3 \cdot 6H_2O$ solution containing 0.05 *N* HCl, whereas the SUS316L stainless steel coating was attacked aggressively.

Keywords amorphous, corrosion resistance, crystallization, HVOF, iron alloy, plasma spraying

1. Introduction

IRON-METALLOID amorphous alloys are unstable chemically compared with pure iron or steels and exhibit a very high corrosion rate. Naka et al. (Ref 1) found that Fe-Cr-P-C amorphous alloys obtained by centrifugal quenching from liquid exhibited higher corrosion resistance than stainless steels in acid or neutral solutions. They also investigated the effect of alloying elements and heat treatment on the corrosion behavior and passive film of Fe-Cr-P-C amorphous alloys containing nickel, molybdenum, and tungsten (Ref 2-5). However, these iron-base amorphous alloys have not been put to practical use as corrosion-resistant materials.

The present authors have investigated the formation and properties of amorphous phases in rapidly solidified high-carbon iron alloys containing chromium and molybdenum in order to develop thermal spray materials of great wear resistance. We have reported that decomposition of the amorphous phase brings about a very high hardness due to the precipitation of fine carbides, although the hardness of the amorphous phase is also high itself (Ref 6-8). High-carbon iron alloys were sprayed by plasma and high-velocity oxyfuel (HVOF) techniques to produce coatings with great wear resistance at high temperature. We have also found that as-sprayed coatings composed of an

K. Kishitake, H. Era, and **F. Otsubo,** Department of Materials Science and Engineering, Faculty of Engineering, Kyushu Institute of Technology, Kita-Kyushu 804, Japan.

Table 1 Spraying conditions

Method	Atmosphere	Current, A	Voltage, V	Oxygen pressure, MPa	Fuel pressure, MPa	Spray distance, mm
LPPS	In chamber (6500 Pa)	1200	60	...	...	300
HVOF	Air	...	...	1.38	1.79	300
HPS	Air	450	430	...	...	200

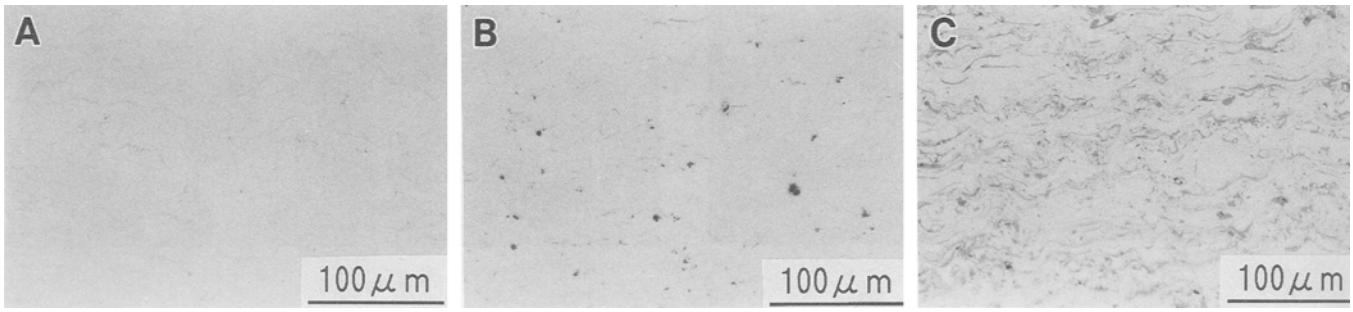

Fig. 1 Optical micrographs of as-sprayed coatings. (a) LPPS. (b) HVOF. (c) HPS

amorphous phase reveal not only high hardness but also higher corrosion resistance than an austenitic stainless steel (JIS-SUS316L) coating in H_2SO_4 solution (Ref 9, 10).

The aim of this study was to investigate the possibility of thermally spraying amorphous alloys having extremely high corrosion resistance. The work was carried out to obtain amorphous coatings of an iron-base alloy with a composition similar to the Fe-Cr-P-C amorphous alloy reported by Naka et al. (Ref 1) by means of three different thermal spraying methods and to investigate the tempering behavior and corrosion resistance of the coatings.

2. Experimental Procedure

Iron-base alloy powders of a given composition of Fe-Cr-P-C were produced using a gas atomization method after melting electrolytic iron, graphite, and ferroalloys in an induction furnace. The chemical composition of the alloy powders was Fe-10.9Cr-13.1P-8.36C-0.77Si (atomic percent). The small amount of silicon was added to prevent oxidation through atomization. Alloy powders smaller than 45 μm in diameter were used for spraying. Coatings about 500 μm thick were obtained on mild steel using (1) 80 kW low-pressure plasma spraying (LPPS), (2) HVOF spraying, and (3) 250 kW high-energy plasma spraying (HPS) under the conditions shown in Table 1.

The coatings were heated under vacuum at various temperatures up to 1073 K for 1 h and air cooled. Structures of the coatings were observed using optical and transmission electron microscopy (TEM). X-ray diffraction (XRD) patterns (Fe-Kα radiation) were also obtained for powders and for as-sprayed and heat-treated coatings. Hardness measurements were carried out using a microhardness tester with a 0.49 N load. Differential thermal analysis (DTA) was performed to study the macroscopic crystallization behavior of the amorphous phase.

Polarization curves were obtained for the as-sprayed and heat-treated coatings to evaluate corrosion resistance using a potentiostat. Deaerated 1 *N* H_2SO_4 and 1 *N* HCl solutions were used for the electrolyte. A platinum counterelectrode and a saturated calomel reference electrode (SCE) were used. The electrochemical measurement of the coatings was carried out by scanning the corrosion potential to +1.1 V (versus SCE) with a scanning rate of 60 mV/min after keeping the potential at –0.7 V (versus SCE) for 10 min at 303 K. Immersion tests were also carried out to confirm the corrosion resistance of the amorphous coatings in two kinds of acid solutions. The coatings were immersed in deaerated 1 *N* HCl solution at 0.5 V (versus SCE) for 1 h at 303 K to investigate the general corrosion behavior and in 6% $FeCl_3 \cdot 6H_2O$ + 0.05 *N* HCl solution at the corrosion potential for 100 h at 308 K to test the pitting corrosion behavior. The coatings were polished with alumina powders of 0.05 μm and were masked with an acid-resistant lacquer to form an exposure area of 1 cm^2 before the electrochemical measurements and immersion tests.

3. Results and Discussion

3.1 *As-Sprayed Coatings*

Figure 1 shows optical micrographs of the as-sprayed coatings. Very thin oxide films are visible, but pores are rarely observed in the LPPS coatings. Only a few pores and very thin

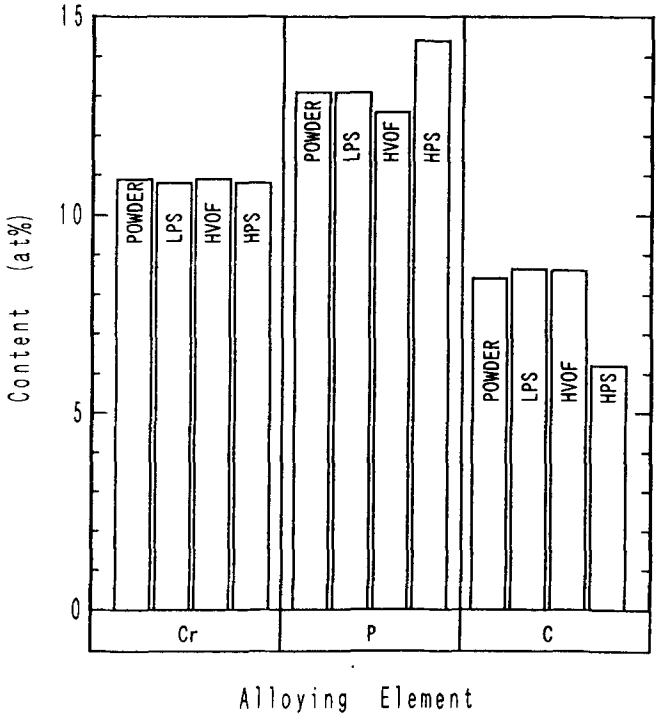

Fig. 2 Change in content of alloying element by thermal spraying

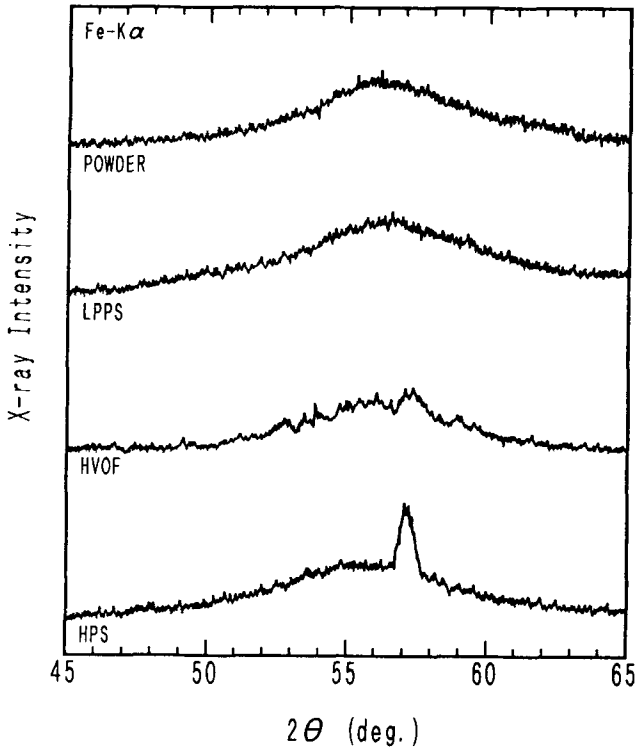

Fig. 3 XRD patterns of powder and as-sprayed coatings

oxide films are contained in the HVOF coatings, and pores and thicker oxide films exist in the HPS coatings.

Chemical analysis of the coatings was carried out to investigate the change in composition produced by the three kinds of thermal spraying processes (Fig. 2). The chemical composition of the LPPS and HVOF coatings was unchanged compared with the powder. The carbon content of the HPS coatings decreased, and the phosphorus content increased slightly as a result of the decrease in carbon.

X-ray diffraction patterns of the powder and the as-sprayed coatings are shown in Fig. 3. Only a broad peak (i.e., a halo pattern) appears for the powder and the LPPS coatings. An amorphous coating is formed by the LPPS process, and a minute quantity of crystalline phases is contained in the HVOF coatings. The HPS coating is composed of a mixture of a small quantity of ferrite phase and an amorphous phase. The difference in the occurrence of crystalline phases may result mainly from differences in the cooling rates of the three processes.

3.2 *Structure and Hardness of Amorphous Coatings on Tempering*

An XRD analysis was carried out to study the crystallization of the amorphous coating by heat treatment at different temperatures for 1 h. Figure 4 shows the results for the LPPS coating. The amorphous phase is retained on tempering up to 673 K. The amorphous phase crystallizes, and the diffraction peaks of α-phase, M_3C carbide, and M_3P phosphide appear on tempering at 773 K. These peaks become sharp on tempering at 973 K. The amorphous phase in the HVOF and HPS coatings also crystallizes at 773 K and forms a mixture of α-phase, M_3C carbide, and M_3P phosphide. Differential thermal analysis curves of the coatings are shown in Fig. 5. The exothermic peaks attributed to crystallization of the amorphous phases are seen in the range of about 740 to 820 K. The exothermic peaks of the HVOF and HPS coatings are lower than that of the LPPS coating because of a smaller volume fraction of the amorphous phase.

Figure 6 shows the effect of tempering on coating hardness. All the as-sprayed coatings exhibit a high hardness of about 700 DPN. The hardness is not changed by tempering up to 673 K. The hardness of all coatings was enhanced by tempering at 773 K because of crystallization of the amorphous phase and reached a maximum of 1000 to 1100 DPN when tempered at 773 or 873 K. The hardness of the HPS coating is low compared with the LPPS and HVOF coatings over the crystallization temperature. The difference is mainly attributable to the difference of volume fraction of the amorphous phase and carbon content in the as-sprayed coatings. The hardness decreases on tempering above 900 K.

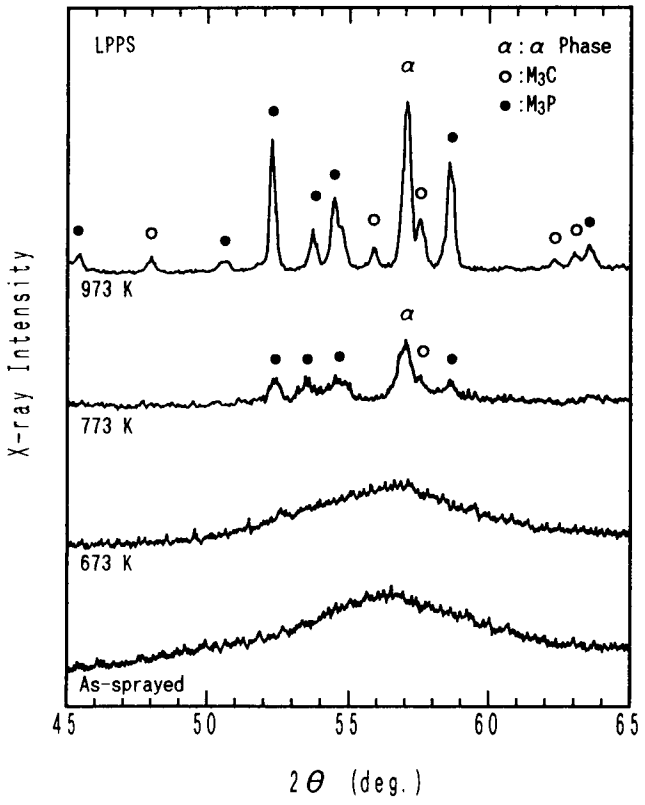

Fig. 4 XRD patterns of coatings tempered at various temperatures

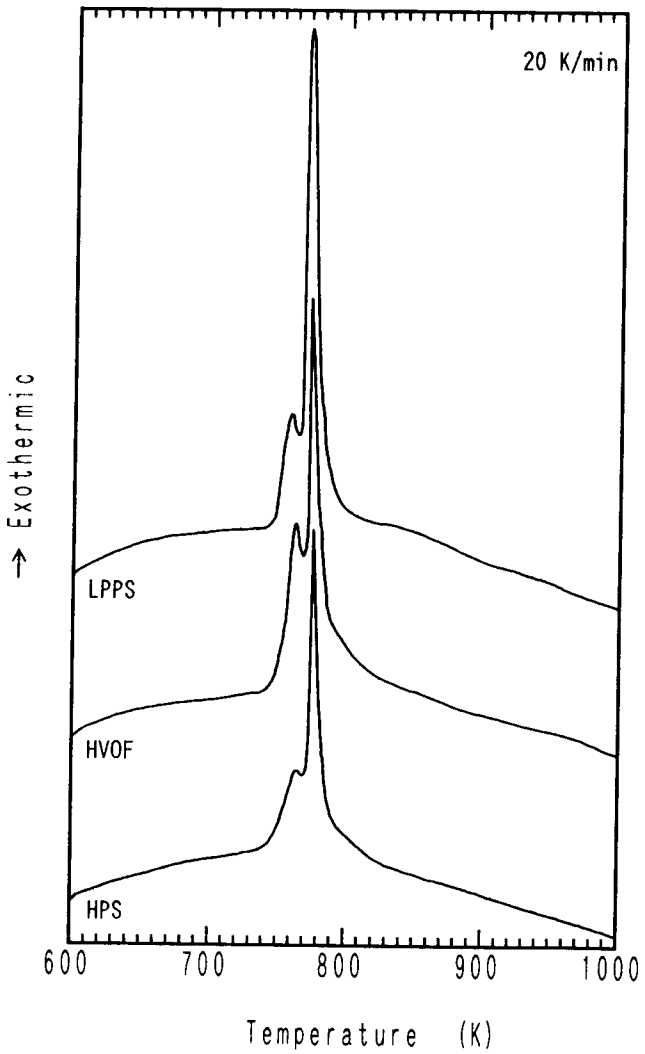

Fig. 5 DTA curves of coatings

Figure 7 shows bright-field TEM images of the LPPS coatings tempered at 873 K (Fig. 7a) and 1073 K (Fig. 7b). Extremely fine equiaxed grains smaller than 0.1 μm in diameter are visible in the coating tempered at 873 K. The coating tempered at 1073 K reveals very fine grains. It is known that a nanostructure is formed by crystallization and remains even after tempering at 1073 K.

3.3 *Corrosion Resistance*

Anodic polarization curves of the as-sprayed and tempered coatings were measured in deaerated 1 N H_2SO_4 solution and 1 N HCl solution at 303 K. Figure 8 shows the results of the as-sprayed coatings obtained by the LPPS, HVOF, and HPS processes in 1 N H_2SO_4 solution. The anodic polarization curve of an 18-8 stainless steel (JIS-SUS316L) coating is also shown for comparison. All the coatings exhibit active-passive transitions. The corrosion potential of the LPPS coating is the highest of these coatings. The difference in corrosion potential among the LPPS, HVOF, and HPS coatings probably is attributable primarily to the presence of crystalline phases and oxide films in the coatings. The current density of the LPPS coating is the lowest of the three tested coatings in the measured potential range. Therefore, the corrosion resistance of the LPPS coating is the best of these coatings. The corrosions resistance of the HPS coating, despite being the worst of the three, is comparable to a SUS316L stainless steel coating.

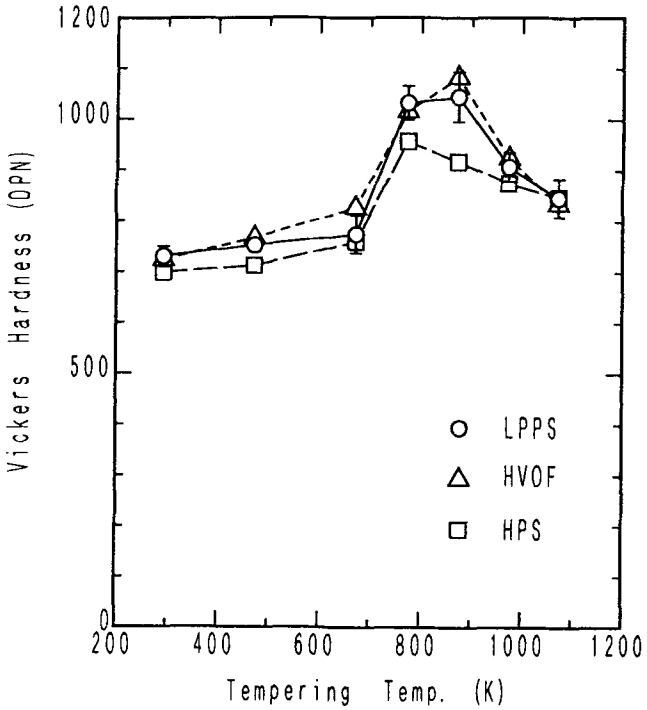

Fig. 6 Change in hardness as a function of tempering temperature. Longitudinal bars at open circles show standard deviation of LPPS coating.

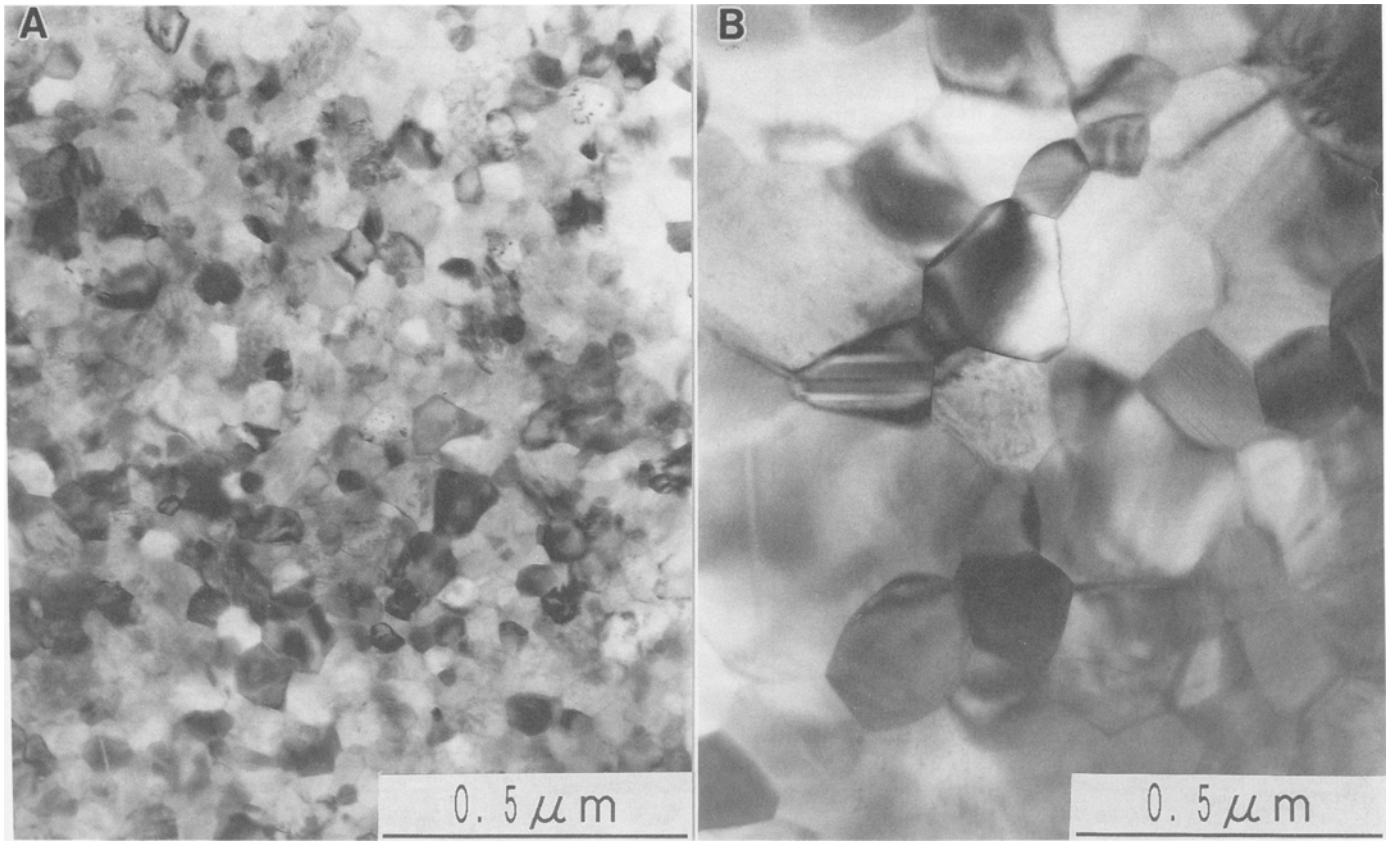

Fig. 7 Bright-field TEM images of coatings by LPPS process tempered at (a) 873 K and (b) 1073 K

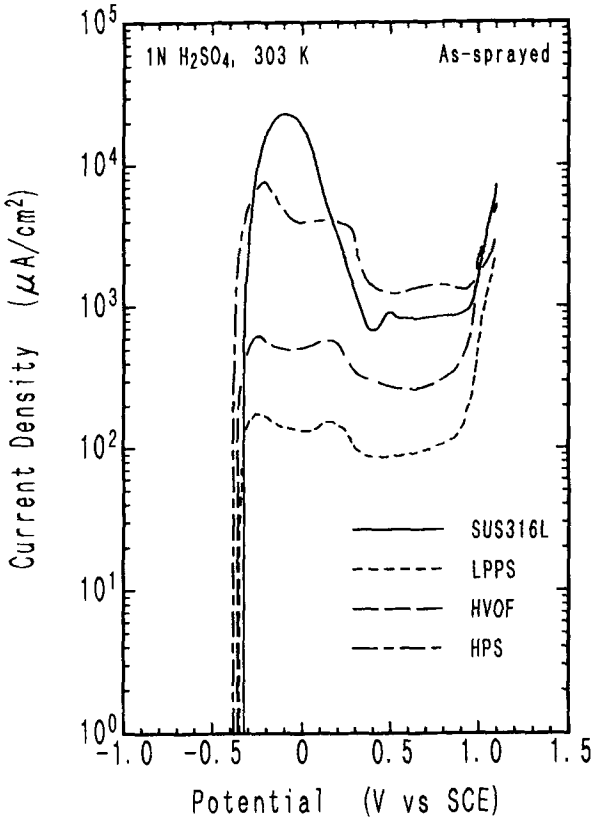

Fig. 8 Anodic polarization curves of as-sprayed coatings

Figure 9 shows anodic polarization curves of the LPPS coating in 1 *N* H_2SO_4 before and after crystallization. The crystallized coatings reveal low corrosion potential and high current densities compared with the as-sprayed amorphous coating. Therefore, the corrosion resistance of the amorphous coating deteriorates with crystallization. However, the corrosion resistance of the crystallized coating is comparable to a SUS316L stainless steel coating.

Figure 10 shows anodic polarization curves of the as-sprayed coatings obtained by the LPPS, HVOF, and HPS processes in 1 *N* HCl. As was the case in 1 *N* H_2SO_4, the corrosion potential of the LPPS coating is the highest and its current density is the lowest. Therefore, the corrosion resistance of the LPPS coating in 1 *N* HCl is also the best of these coatings. Furthermore, the LPPS coating possesses higher corrosion resistance in 1 *N* HCl than in 1 *N* H_2SO_4. This result can be contrasted with a SUS316L stainless steel coating, which exhibits a high anodic current density in 1 *N* HCl. When compared with the electrochemical measurement results of an amorphous alloy ribbon (Ref 1), which has a composition similar to this work, the corrosion potential of the LPPS coating is lower than the ribbon and the current densities are higher by about one order of magnitude than that of the ribbon in 1 *N* H_2SO_4. The LPPS coating shows an active and passive state in 1 *N* HCl, whereas the ribbon shows a self-passivation in the anodic polarization curves (Ref 3). Thus, the passivation behavior differs between the coating and ribbon, although the amorphous alloys have a similar composition. This may be due to the existence of oxide films in the sprayed coat-

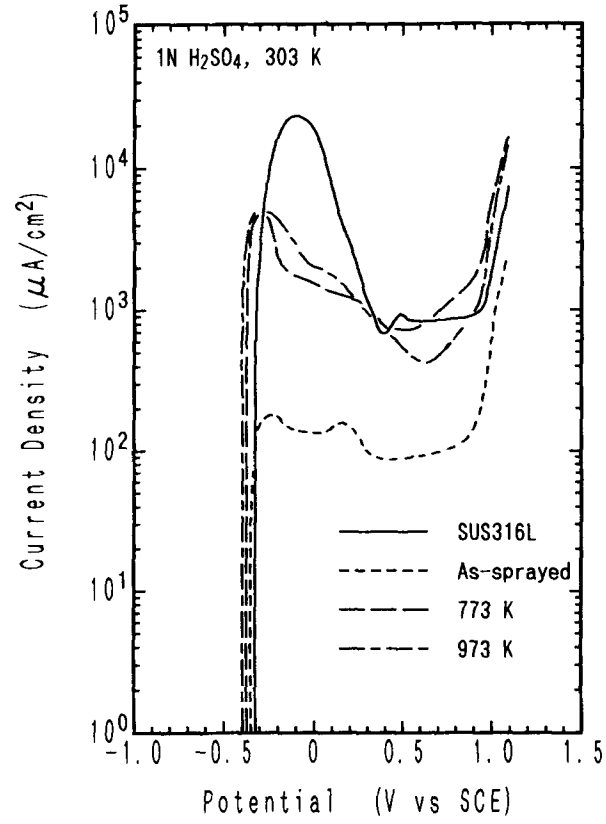

Fig. 9 Anodic polarization curves of LPPS coatings

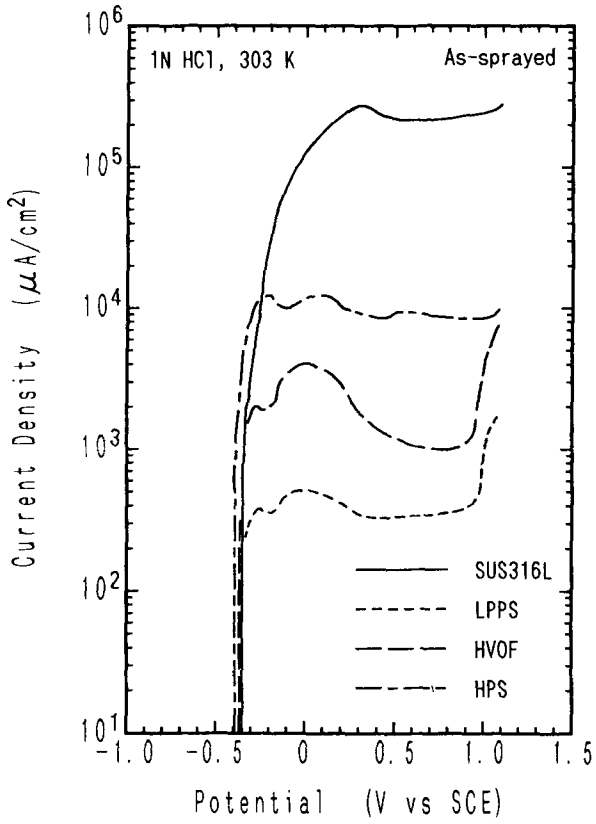

Fig. 10 Anodic polarization curves of as-sprayed coatings

ing. It is thus expected that the amorphous coating would passivate spontaneously in acidic chloride environments if free from oxide films.

Immersion tests were performed to confirm coating corrosion resistance in 1 *N* HCl solution at 0.5 V (versus SCE) and 6% $FeCl_3 \cdot 6H_2O$ solution containing 0.05 *N* HCl at the corrosion potential. Figure 11 shows the cross sections of the coatings where the top part is of the polished exposure surface. Photographs A to C are the cross sections of the coatings before immersion, and D to F are the cross sections after immersion in 1 *N* HCl solution at 0.5 V for 15 min (D) and 1 h (E and F). It is clear that the SUS316L stainless steel coating (D) corrodes over 100 μm depth after immersion in 1 *N* HCl for 15 min. In contrast, preferential attack occurs slightly through oxide films near the surface in the HPS coating (E), and the LPPS coating (F) is not attacked at all. These results are in fair agreement with the electrochemical measurement results.

Photographs G to I in Fig. 11 show the cross sections after immersion in 6% $FeCl_3 \cdot 6H_2O$ + 0.05 *N* HCl solution at corrosion potential for 10 h (G) and 100 h (H and I). This solution is conventionally used for the pitting corrosion test of stainless steel. The SUS316L stainless steel coating (G) is attacked aggressively in 10 h. Internal corrosion occurs partially in the HPS coating after immersion for 100 h, but the extent of corrosion is fairly low compared with the SUS316L coating immersed for 10 h. On the other hand, neither general corrosion nor pitting takes place in the LPPS coating after immersion for 100 h as well as the immersion test in 1 *N* HCl. These results indicate that the amorphous coating possesses better corrosion resistance than other iron-base alloy coatings in acidic solutions for the test conditions.

4. Conclusions

The Fe-10Cr-13P-7C alloy powders were thermally sprayed by 80 kW LPPS, HVOF, and 250 kW HPS. The tempering behavior and corrosion resistance of the coatings were investigated. The results can be summarized as follows:

- An amorphous coating is obtained by the LPPS process, and a mixture of amorphous and crystalline phases is

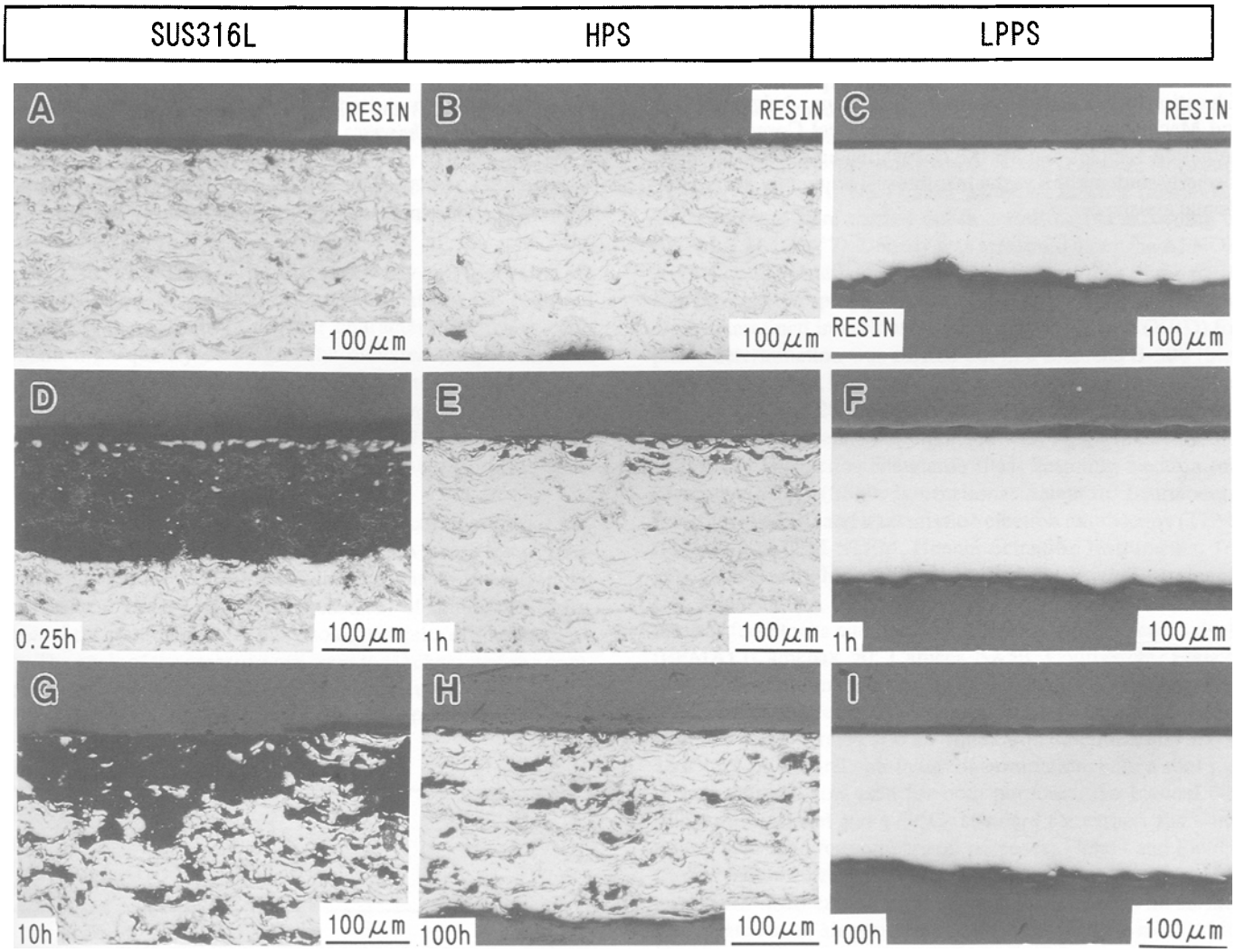

Fig. 11 Optical micrographs of coatings before and after immersion test in various conditions. A to C, before immersion; D to F, after immersion in 1 *N* HCl solution at 0.5 V; G to I, after immersion in 6% $FeCl_3$ $6H_2O$ solution containing 0.05 *N* HCl

formed in the HVOF and HPS coatings. The as-sprayed coatings show a high hardness of greater than 700 DPN.

- The amorphous phase in the coatings crystallizes at about 740 K. The LPPS coating shows a maximum hardness of 1050 DPN just after crystallization. This high hardness is attributable to the very fine structure composed of α-phase, M_3C carbide, and M_3P phosphide.

- The corrosion resistance of the amorphous LPPS coating is the best of the three coatings and superior to a SUS316L stainless steel coating in 1 *N* H_2SO_4 and 1 *N* HCl solutions. The amorphous coating also shows outstanding corrosion resistance compared with the SUS316L stainless steel coating in 1 *N* HCl solution at 0.5 V (versus SCE) and 6% $FeCl_3 \cdot 6H_2O$ solution containing 0.05 *N* HCl at the corrosion potential.

The amorphous LPPS coating is expected to have good wear resistance and excellent corrosion resistance in acidic chloride environments.

Acknowledgments

This work was supported by a grant-in-aid of the Ministry of Education in Japan. The authors wish to acknowledge the Plant and Machinery Division of the Nippon Steel Corporation for preparing samples and Mr. K. Nakashima and Mr. T. Kichise, formerly students of Kyushu Institute of Technology, for experimental assistance.

References

1. M. Naka, K. Hashimoto, and T. Masumoto, Corrosion Resistivity of Amorphous Iron Alloys Containing Chromium, *J. Jpn. Inst. Met.*, Vol 38, 1974, p 835-841 (in Japanese)
2. K. Hashimoto, K. Osada, T. Masumoto, and S. Shimodaira, Characteristics of Passivity of Extremely Corrosion-Resistant Amorphous Iron Alloys, *Corros. Sci.*, Vol 16, 1976, p 71-76
3. M. Naka, K. Hashimoto, and T. Masumoto, Effect of Heat Treatment on Corrosion Behavior of Amorphous Fe-Cr-P-C and Fe-Ni-Cr-P-B Alloys in 1 *N* HCl, *Corrosion*, Vol 36, 1980, p 679-686
4. H. Habazaki, A. Kawashima, K. Asami, and K. Hashimoto, The Effect of Tungsten on the Corrosion Behavior of Amorphous Fe-Cr-W-P-C Alloys in 1 *M* HCl, *J. Electrochem. Soc.*, Vol 138, 1991, p 76-81
5. H. Habazaki, A. Kawashima, K. Asami, and K. Hashimoto, The Corrosion Behavior of Amorphous Fe-Cr-Mo-P-C and Fe-Cr-W-P-C Alloys in 6 *M* HCl Solution, *Corros. Sci.*, Vol 33, 1992, p 225-236
6. K. Kishitake, H. Era, and F. Otsubo, Enhancement of Hardness by Heat Treatment in Rapidly Solidified High-Carbon Iron Alloys, *Scr. Metall. Mater.*, Vol 24, 1990, p 1269-1273
7. K. Kishitake, H. Era, F. Otsubo, P. Li, and N. Wakayama, Tempering Behavior of Rapidly Solidified Eutectic High-Carbon Fe-Cr-Mo-B Alloys, *J. Jpn. Foundrymen's Soc.*, Vol 65, 1993, p 468-473 (in Japanese)
8. K. Kishitake, H. Era, F. Otsubo, and T. Hasegawa, Effect of C/B Ratio on Crystallization and Hardness of Eutectic Fe-Cr-Mo Amorphous Alloys, *J. Jpn. Foundrymen's Soc.*, Vol 67, 1995, p 613-618 (in Japanese)
9. K. Kishitake, H. Era, and F. Otsubo, Characterization of Plasma-Sprayed Fe-10Cr-10Mo-(C,B) Amorphous Coatings, *J. Therm. Spray Technol.*, Vol 5, p 145-153
10. K. Kishitake, H. Era, and F. Otsubo, Characterization of Plasma-Sprayed Fe-17Cr-38Mo-4C Amorphous Coatings Crystallizing at Extremely High Temperature, *J. Therm. Spray Technol.*, Vol 5, p 283-288